Piezoelectric anisotropy and energy-harvesting characteristics of novel sandwich layer $BaTiO_3$ structures

James I Roscow[1], Vitaly Yu Topolov[2,3], John T Taylor[4] and Christopher R Bowen[1]

[1]Materials and Structures Centre, Department of Mechanical Engineering, University of Bath, Bath BA2 7AY, UK

[2]Department of Physics, Southern Federal University, 344090 Rostov-on-Don, Russia

[3]Institute of High Technologies and Piezotechnics, Southern Federal University, 344090 Rostov-on-Don, Russia

[4]Department of Electronic and Electrical Engineering, University of Bath, Bath BA2 7AY, UK

E-mail: vutopolov@sfedu.ru

Received 6 May 2017, revised July 2017

Abstract

This paper presents a detailed modelling and experimental study of the piezoelectric and dielectric properties of novel ferroelectric sandwich layer $BaTiO_3$ structures that consist of an inner porous layer and dense outer layers. The dependencies of the piezoelectric coefficients d_{3j}^* and dielectric permittivity $\varepsilon_{33}^{*\sigma}$ of the sandwich structure on the bulk relative density α are analysed by taking into account an inner layer with a porosity volume fraction of 0.5–0.6. The observed changes in d_{3j}^* and $\varepsilon_{33}^{*\sigma}$ are interpreted within the framework of a model of a

laminar structure whereby the electromechanical interaction of the inner porous layer and outer dense layers have an important role in determining the effective properties of the system. The porous layer is represented as a piezocomposite with a 1–3–0 connectivity pattern, and the composite is considered as a system of long poled ceramic rods with 1–3 connectivity which are surrounded by an unpoled ceramic matrix that contains a system of oblate air pores (3–0 connectivity). The outer monolithic is considered as a dense poled ceramic, however its electromechanical properties differ from those of the ceramic rods in the porous layer due to different levels of mobility of 90° domain walls in ceramic grains. A large anisotropy of d_{3j}^* at α= 0.64–0.86 is achieved due to the difference in the properties of the porous and monolithic layers and the presence of highly oblate air pores. As a consequence, high energy-harvesting figures of merit $d_{3j}^* g_{3j}^*$ are achieved that obey the condition $d_{33}^* g_{33}^*/(d_{31}^* g_{31}^*)\sim 10^2$ at $d_{33}^* g_{33}^* \sim 10^{-12}$ Pa^{-1}, and values of the hydrostatic piezoelectric coefficients $d_h^* \approx$ 100 pC / N and $g_h^* \approx$ 20 mV·m / N are achieved at α= 0.64–0.70. The studied $BaTiO_3$-based sandwich structures has advantages over highly anisotropic $PbTiO_3$-type ceramics as a result of the higher piezoelectric activity of ceramic $BaTiO_3$ and can be used in piezoelectric sensor, energy-harvesting and related applications.

Keywords: Piezoelectric properties, anisotropy, porous ferroelectrics, energy-harvesting figures of merit, dielectric permittivity.

1. Introduction

Interest in the development of new porous ferroelectric materials and their applications [1–7] has arisen for a number of reasons. Firstly, when porous ferroelectric ceramics (FCs) with a perovskite-type structure are in a poled state, they exhibit piezoelectric properties [4–9] that are of value for piezotechnical and related transducer applications. Secondly, the microgeometry–properties relations in these porous materials are complex [6, 8, 9] and can be affected by a variety of conditions related to their manufacture, poling and mechanical properties [1–4]. Thirdly, the opportunity to manufacture novel ferroelectric materials with a specific microgeometry of air pores [1–3, 10, 11] enables researchers to tailor the effective electromechanical properties and their anisotropy [8, 9]. Fourthly, different methods [8, 11–16] can be applied*) to predict the effective properties of the porous material and features of its poling. Finally, in the last decade, the desire to produce high-performance lead-free FCs and improve their electromechanical properties [17–19] has become an important stimulus to manufacture novel porous

---

*) Effective electromechanical properties of porous ferroelectric materials can be calculated, for instance, within the framework of the theoretical approach [12] based on the micromechanical model wherein the electromechanical coupling in the piezoelectric medium and the pore shape are taken into account. The full set of electromechanical constants of the porous material can also be evaluated using analytical formulae [11, 15], by consecutively applying the methods [8, 12, 13] concerned with micromechanical models and specifics of the composite microgeometry, and by the finite element method [14, 16]. In work [14] an incomplete poling of porous samples is also taken into account. The finite element multi-inclusion modelling of piezocomposites [16] that contain a few components is also promising for an analysis of porous materials with a complex microgeometry.

piezoelectric materials [5–7] and structures with improved characteristics.

Recently, a novel porous sandwich layer (PSL) $BaTiO_3$ has been put forward [7] as a new kind of porous lead-free material that can be applied in piezoelectric transducers, energy harvesters and sensors. However in Ref. 7 only limited characteristics related to the longitudinal piezoelectric effect are discussed, and no data on the lateral piezoelectric effect, anisotropy of the piezoelectric coefficients d_{3j}^* and related parameters are reported. The aims of the present paper are (i) to study the piezoelectric and dielectric properties and figures of merit (FOMs) of novel PSL $BaTiO_3$ with an inner layer with a porosity volume fraction of 0.5–0.6 and (ii) to highlight the density ranges whereby a large piezoelectric anisotropy is observed in these structures.

2. Manufacturing of porous sandwich layers and experimental results

PSL $BaTiO_3$ samples were manufactured by alternatively layering prepared barium titanate starting powders containing varying fractions of pore forming agent before uniaxial pressing and sintering. For the dense outer layers, the starting powder was prepared from commercial barium titanate powder (*Ticon P, Ferro,* UK) and 5 wt.% organic binder, polyethylene glycol (PEG) (*Sigma*, UK), which was ball milled with zirconia milling media and distilled water for 24 h prior to drying, regrinding and sieving through a 150 μm mesh. The starting powder for the porous inner layer was produced from dry mixing barium titanate with PEG in varying quantities (25 and 35 wt. %) so as to achieve different inner layer porosities. The

powders were sequentially layered into a uniaxial tablet die with layers gently flattened before the next was layer added, before being pressed at 185 MPa to form the green pellets. The pellets were sintered in air at 1300°C for 2 h with a heating/cooling rate of 60°C / h, and a two-hour dwell stage was included at 400°C to burn off the organic binder/pore forming agent. The sintered pellets were cleaned, and their densities measured via the Archimedean method. Silver electrodes were painted onto the samples (*RS Components, Product No 186-3600*) prior to corona poling at 14 kV at a distance of 35 mm from the samples, at a temperature of 115°C.

The piezoelectric properties, namely, piezoelectric coefficients d^*_{3j}, were measured using a *Take Control Piezometer PM25* at 97 Hz. Impedance spectroscopy (*Solartron 1260* and *1296 Dielectric Interface*, *Solartron Analytical*, UK) was used to measure the dielectric properties of the samples allowing calculation of the relative permittivity. Scanning electron microscopy was used to investigate the PSL structure and measure the inner porosity p_{in} in the porous layer. An optical micrograph of the outer surface of the PSL $BaTiO_3$ sample is shown in figure 1(a). Samples produced with high fractions of pore-forming agent in the PSL demonstrated excellent cohesion between layers, although some inter-layer cracks perpendicular to the poling direction were occasionally observed in SEM images. These tended to be smaller than the pore size and therefore not thought to significantly influence the measured properties. Sequential pressing of layers also resulted in the PSL exhibiting a small slant with respect to the poling direction in

some samples, as can be seen in figure 1(a); a processing technique such as tape casting would likely be able to produce PSL materials with more consistent layering.

Experimental data showing the changes in the piezoelectric coefficients d^*_{3j} and dielectric permittivity $\varepsilon^{*\sigma}_{33}$ at mechanical stress σ = constant with the relative density α of the PSL are represented in figure 2 for two levels of the inner layer porosity (p_{in}); lower porosity fractions were difficult to achieve using the fabrication method discussed here due to inter-layer cracks forming during pressing and sintering. Hereafter we denote the samples PSL-1 and PSL-2 for $p_{in} \approx$ 0.5 and 0.6, respectively. It is seen that the piezoelectric coefficients d^*_{3j} [figure 2(a)] obey the condition

$$d^*_{33}/|d^*_{31}| \approx 10 \qquad (1)$$

at $d^*_{33} \approx$ (90–130) pC /N and the relative permittivity level $\varepsilon^{*\sigma}_{33}/\varepsilon_0 \sim 10^2$–$10^3$ [figure 2(b)]. The studied PSL material has advantages over the highly anisotropic $PbTiO_3$-type FCs [20] with a large anisotropy of d^*_{3j} due to the lead-free nature of the PSL and the d^*_{33} values being about twice larger than d_{33} of the $PbTiO_3$-type FCs. From the experimental results shown in figure 2, a large piezoelectric coefficient $g^*_{33} = d^*_{33} / \varepsilon^{*\sigma}_{33}$ is achieved due to the relatively small dielectric permittivity $\varepsilon^{*\sigma}_{33}$. For instance, at a relative density $\alpha = 0.653$ for PSL-2, $g^*_{33} = 30.2$ mV·m / N, and at $\alpha = 0.698$ for PSL-1, $g^*_{33} = 21.3$ mV·m / N. This is in contrast to

the piezoelectric sensitivity of the monolithic poled $BaTiO_3$ FC [21] which is characterised by a piezoelectric coefficient g_{33} = 12.6 mV·m / N at room temperature. Due to the relatively large values of the piezoelectric coefficient d^*_{33} ~ 10^2 pC / N of the PSL in a wide α range [figure 2(a)], the order-of-magnitude of the energy-harvesting FOM

$$(Q^*_{33})^2 = d^*_{33}\, g^*_{33} \qquad (2)$$

(or the squared FOM concerned with the longitudinal piezoelectric effect) is typically 10^{-12} Pa^{-1}. As is known, the FOM from Eq. (2) is proportional to the 'signal – noise' ratio [8] for a piezoelectric transducer at the longitudinal oscillation mode. The squared FOM concerned with the transverse piezoelectric effect of the PSL sample is

$$(Q^*_{31})^2 = d^*_{31}\, g^*_{31} \qquad (3)$$

and small in comparison to $(Q^*_{33})^2$ from Eq. (2) while Eq. (1) is valid for the studied PSL material.

The large piezoelectric anisotropy observed in the novel PSL $BaTiO_3$ leads to an increase of the hydrostatic piezoelectric coefficients $d^*_h = d^*_{33} + 2\, d^*_{31}$ and $g^*_h = g^*_{33} + 2\, g^*_{31}$ when compared to the d_h and g_h parameters of the monolithic counterpart. Moreover, an increase of g^*_h of the PSL compared to the monolithic g_h is also a result of the dielectric properties that strongly depend on porosity v_p of the PSL structure. Examples of the experimental dependence of the piezoelectric coefficients on the bulk relative density $\alpha = 1 - v_p$ are given in Table 1. According

to experimental data [21], the monolithic poled $BaTiO_3$ FC is characterised by hydrostatic piezoelectric coefficients d_h = 34 pC / N and g_h = 2.26 mV·m / N. As follows from measurements on the monolithic poled $BaTiO_3$ FC samples in the present study, their piezoelectric coefficients are d_{33} = 124.8 pC / N and d_{31} = –47.8 pC / N and relative dielectric permittivity at 1 kHz is $\varepsilon_{33}^{\sigma} / \varepsilon_0$ = 1504 (average values). This means that the hydrostatic piezoelectric coefficients are d_h = 29.2 pC / N and g_h = 2.19 mV·m / N, i.e., in agreement with the hydrostatic parameters from Ref. 21. For the studied PSL samples, the typical ratios $d_h^* / d_h \approx$ 2–3 and $g_h^* / g_h \approx$ 4.1–9.5 are achieved, see experimental values in Table 1.

3. Modelling and interpretation of the piezoelectric and dielectric properties of the PSL $BaTiO_3$

Recently, the modelling of the longitudinal piezoelectric response of the PSL $BaTiO_3$ [7] showed that incomplete poling of the porous ferroelectric material had a strong influence on its piezoelectric activity and related parameters. Our current efforts are concentrated on describing the piezoelectric and dielectric properties of PSL materials by taking into account features of their porosity and domain-wall mobility in their FC grains and to interpret the influence of microgeometric factors on the piezoelectric anisotropy.

The PSL structure is assumed to contain porous and monolithic FC layers poled along the co-ordinate OX_3 axis, see figure 1(b). In the porous layer, the FC matrix contains isolated spheroidal air pores, see the inset of figure 1(b). It is

assumed that these pores are regularly distributed in the porous layer of the PSL. The shape of the air pore is described by the equation $(x_1 / a_{1p})^2 + (x_2 / a_{2p})^2 + (x_3 / a_{3p})^2 = 1$ relative to the axes of the co-ordinate system ($X_1X_2X_3$), where the semiaxes of the pore are $a_{1p} = a_{2p}$ and a_{3p}, and $\rho_p = a_{1p} / a_{3p}$ is its aspect ratio. The porous matrix shown in the inset in figure 1(b) is described by 3–0 connectivity in terms of work by Newhnam et al. [22]. This porous matrix is reinforced by a system of monolithic FC rods that are oriented along the OX_3 axis. This particular orientation of the FC rods facilitates their poling under an applied electric field $\boldsymbol{E} \parallel OX_3$ and promotes an effective electromechanical coupling between the layers that are shown in figure 1(b). We assume that each FC rod is in the form of a long circular cylinder which is characterised by a considerable mobility of the 90° domain walls in each FC grain in the poled state. The porous matrix surrounding the monolithic FC rods leads to a decrease of the mechanical stress during the 90° domain switching and can be regarded as an additional argument for the considerable domain-wall mobility. Changes in the parameters m_p and ρ_p of the porous matrix enable us to vary the elastic anisotropy of the matrix and porous layer as a whole. This factor influences [8, 13] the piezoelectric properties and their anisotropy in the PSL structure.

The porous layer shown in figure 1(b) is characterised by 1–3–0 connectivity, and its electromechanical properties depend on the volume fractions r and m_p and domain-wall mobility in the FC rods. The outer monolithic layer of the PSL sample is represented by the same FC, but with a lower domain-wall mobility in FC grains

in comparison to the domain-wall mobility in the FC-rod grains. This lower domain-wall mobility may be a result of the perpendicular orientation of the monolithic layer with respect to the poling direction OX_3, see figure 1(b).

The 90° domain-wall mobility in the FC grains can be taken into account in terms of work [23]. According to Aleshin [23], it is assumed that during the poling stage of the FC sample, the 180° domains are removed. As a result, each grain is assumed to be split into the 90° domains that are separated by planar walls, and the 90° domain-wall displacements are caused by an external field, which is either electric or stress based. The electromechanical properties of the poled FC depend on $\lg \gamma$ that characterises the mobility of the 90° domain walls, where $\gamma = (Hc)^{-1} \cdot 10^{-6}$ Pa, H is the average width of the 90° domain, and c links the domain-wall displacement x and thermodynamic pressure f in accordance with the linear relation $f = cx$. Full sets of electromechanical constants of the monolithic poled $BaTiO_3$ FC were calculated by Aleshin [23] in the range $-4 \le \lg \gamma \le 4$. The value of $\lg \gamma = -4$ corresponds to almost immovable 90° domain walls in the FC grain, and at $\lg \gamma = 4$ the highest mobility of the 90° domain walls is expected. At $-4 \le \lg \gamma \le 0$, an appreciable increase of elastic compliances $|s_{ab}^{E}|$, piezoelectric coefficients $|d_{ij}|$ and dielectric permittivities $\varepsilon_{pp}^{\sigma}$ is observed. For instance, the piezoelectric coefficient d_{33} of the poled $BaTiO_3$ FC monotonously increases from –75 to 158 pC / N. At $0 < \lg \gamma \le 4$, the properties of the poled $BaTiO_3$ FC undergo smaller changes [23][#]),

---

[#]) It should be added that the concepts [23] were highlighted in work [24] on the 1–3-type FC / auxetic polymer composites and their piezoelectric performance. The full sets of electromechanical constants of the poled $BaTiO_3$ FC at $-4 \le \lg\gamma \le 4$ [23] were first applied [24] to find the piezoelectric coefficients d_{33}^* and g_{33}^*, and their hydrostatic analogs g_{33}^* and g_h^* of the 1–3-type composites. These parameters undergo minor changes at $0 < \lg\gamma \le 4$ in FC grains and at constant volume fractions of the FC component in the composite.

e.g. $d_{33} \approx 160$ pC / N.

The prediction of the effective electromechanical properties and energy-harvesting FOMs from Eqs. (2) and (3) is carried out in three stages as follows. In the first stage, the effective properties of the porous 3–0 non-poled FC matrix [see the inset in figure 1(b)] are evaluated as a function of m_p and ρ_p within the framework of the dilute approach [6, 12], and an interaction between the air pores is neglected. The matrix of the effective properties of the medium with spheroidal air pores is written as

$$|| C^{(m)} || = || C^{(1)} || [|| I || - m_p(|| I || - (1 - m_p)|| S ||)^{-1}]. \quad (4)$$

In Eq. (4) $|| C^{(1)} ||$ is the 9×9 matrix that describes the properties of the monolithic FC, $|| I ||$ is the 9×9 identity matrix, $|| S ||$ is the 9×9 matrix containing components of the Eshelby electroelastic tensor [8, 25], and m_p is the volume fraction of the air pores, see the inset in figure 1(b). Elements of $|| S ||$ depend [25] on the aspect ratio ρ_p of the air pore and on the properties of the monolithic FC medium that surrounds the pores. The $|| C^{(1)} ||$ matrix from Eq. (4) is given by

$$|| C^{(1)} || = \begin{pmatrix} || c^{(1),E} || & || e^{(1)} ||^t \\ || e^{(1)} || & - || \varepsilon^{(1),\xi} || \end{pmatrix}, \quad (5)$$

where $\| c^{(1),E} \|$ is the 6×6 matrix of elastic moduli measured at E = constant, $\| e^{(1)} \|$ is the 6×3 matrix of piezoelectric coefficients, and $\| \varepsilon^{(1),\xi} \|$ is the 3×3 matrix of dielectric permittivities measured at mechanical strain ξ = constant. The superscript t in Eq. (5) denotes the transposition. Because of our assumption on the non-poled FC matrix in the porous layer of the PSL structure, the $\| e^{(1)} \|$ and $\| e^{(1)} \|^t$ matrices from Eq. (5) contain zero elements only. The $\| C^{(m)} \|$ matrix from Eq. (4) has the form shown in Eq. (5).

In the second stage, the effective (averaged) properties of the porous layer of the PSL structure are evaluated using the effective field method [8]. In this case we consider the electromechanical interaction between the monolithic FC rods, and the effective properties of the porous layer as a whole (1–3–0 composite) depend on the volume fraction r of the monolithic FC rods and parameter m_p and ρ_p of the porous matrix that surrounds these rods. The evaluation of the effective properties of the porous layer is carried out on assumption that the linear sizes of each pore are much smaller than the radius of the FC rod, i.e., the system of FC rods is surrounded by the porous medium with a set of effective constants. The effective properties of the porous layer are represented in accordance with the effective field method as

$$\| C^{(pl)} \| = \| C^{(m)} \| + r(\| C^{(FC)} \| - \| C^{(m)} \|)\,[\| I \| + (1-r)\,\| S^{(m)} \|\,\| C^{(m)} \|^{-1}(\| C^{(FC)} \| - \| C^{(m)} \|)]^{-1}. \quad (6)$$

In Eq. (6) the matrices of the properties $\| C^{(FC)} \|$ (poled FC rods) and $\| C^{(m)} \|$ [porous non-poled FC matrix, see figure 1(b)] have the form shown in Eq. (5), r is the volume fraction of the poled FC rods in the porous layer of PSL material, $\| I \|$ is the

identity matrix, and $\| S^{(m)} \|$ is the matrix that contains components of the Eshelby electroelastic tensor [25] of the non-poled porous FC medium. Elements of $\| S^{(m)} \|$ depend on the shape of the FC rod and on the properties of the porous FC medium that surrounds each FC rod.

The third stage is concerned with averaging of the properties of the monolithic and porous layers on the volume fraction m [see figure 1(b)], and during this averaging, we take into account the electromechanical interaction between the piezo-active layers and boundary conditions [8] for mechanical and electric fields at the interface $x_3 =$ constant [see figure 1(b)]. The boundary conditions at $x_3 =$ constant imply a continuity of components of mechanical stress σ_{13}, σ_{23} and σ_{33}, strain ξ_{11}, ξ_{12} and ξ_{22}, electric displacement D_3, and electric field E_1 and E_2. Thus, the effective electromechanical properties of the PSL sample shown in figure 1(b) are given by the $\| C^* \|$ matrix that depends on m_p, ρ_p, r, m, lg γ_1, and lg γ_2, where γ_1 refers to the domain-wall mobility in grains of the FC rod, and γ_2 refers to the domain-wall mobility in grains of the monolithic FC layer. The $\| C^* \|$ matrix has the form shown in Eq. (5) so that the PSL FC is characterised by the following electromechanical constants: c_{ab}^{*E}, e_{ij}^{*} and $\varepsilon_{vv}^{*\xi}$. Taking the parameters from figure 1(b) into account, we represent the relative bulk density of the PSL sample as $\alpha = 1 - (1 - r)mm_p$. A transition from the effective piezoelectric coefficients e_{ij}^{*} to d_{ij}^{*} and g_{ij}^{*} is carried out by using conventional formulae [26] for the piezoelectric medium.

Results of our evaluations are shown in figures 3–5 and Tables 1 and 2. In general, the graphs from figure 3 are consistent with the experimental $d_{3j}^{*}(\alpha)$ dependence shown in figure 2(a). Hereby the porous layer of PLS is characterised by an inner layer porosity $p_{in} = (1 - r)m_p$, see figure 1(b). At $m_p = 0.6$ we obtain $p_{in} = 0.54$, 0.51 and 0.48 for $r = 0.10$, 0.15 and 0.20, respectively, and these p_{in} values can correspond to PSL-1. At $m_p = 0.7$ we have $p_{in} = 0.63$, 0.595 and 0.56 for $r = 0.10$, 0.15 and 0.20, respectively, and these p_{in} values can correspond to PSL-2. The graphs in figure 3 suggest that even relatively small changes in the volume fraction r of the poled FC rods in the porous layer can lead to the distinct changes in the piezoelectric coefficients d_{3j}^{*} of the PSL $BaTiO_3$ and also influence the anisotropy of d_{3j}^{*}. On increasing r, the anisotropy of d_{3j}^{*} becomes smaller, and this trend is caused by the small anisotropy of d_{3j} of the monolithic $BaTiO_3$ FC at various values of γ. In the present study, we consider the situation when the 90° domain-wall mobility in the grains of the FC rods is more than that in the monolithic layer of PSL, i.e., the condition $\gamma_1 > \gamma_2$ holds. Comparing figure 3(a) to figure 3(c) and figure 3(b) to figure 3(d), we see that the anisotropy of d_{3j}^{*} becomes smaller on decreasing the aspect ratio ρ_p of the air pore. This decrease strongly influences the elastic properties of the porous FC matrix shown in the inset of figure 1(b) and leads to changes in the piezoelectric coefficients d_{3j}^{*} of the PSL $BaTiO_3$. The mutual arrangement of curves 1–3 (piezoelectric coefficient d_{33}^{*}) in figure 3(b) differs from the arrangements in the remaining graphs of figure 3. This

can be accounted for by a specific competition of the piezoelectric properties of the porous and monolithic layers at a relatively small difference between the piezoelectric coefficients d_{33} of these layers. The competition is related to the PSL where the matrix porosity level is high (m_p = 0.7) and the pores are highly oblate (ρ_p = 100). Such a porous structure leads to a large elastic anisotropy that also influences the piezoelectric properties of the porous layer and PSL structure as a whole. A simple comparison of figure 3(a) and (b) enables us to state that for the smaller matrix porosity m_p = 0.6, a crossing of the curves 1–3 is also observed, but at higher relative densities α of the PSL structure compared to m_p = 0.7. We observe minor changes of the d_{33}^* values [cf. curves 1–3 in figure 3(a) and (b)], and therefore, the aforementioned competition of the piezoelectric properties of the layers is effective.

The graphs in figure 4 show that the evaluated $\varepsilon_{33}^{*\sigma}(\alpha)$ dependence correlates with the experimental data from figure 2(b), however there are differences between the calculated and experimental $\varepsilon_{33}^{*\sigma}$ values. The main reason for these differences is the regular porous structure at m_p = constant and ρ_p = constant, see the inset in figure 1(b). The next reason may be concerned with features of the monolithic poled FC rods and their regular arrangement in the porous matrix: in the present study we consider the system of the long cylindrical FC rods oriented parallel to the poling axis only. The interfaces that separate the monolithic and porous layers in the PSL sample are planar [see figure 1(b)], however any deviation from the

ideal planar interface could lead to changes in the electromechanical coupling between the layers and influence the piezoelectric and dielectric properties of the PSL sample as a whole. It should be added that recently, Wang et al. [27] studied sandwich-structured polymer $BaTiO_3$-based composites wherein the interfaces between adjacent layers strongly influence the dielectric properties, breakdown strength and other characteristics of these materials. A minor reason for the differences between the calculated and experimental $\varepsilon_{33}^{*\sigma}$ values [see figures 2(b) and 4] consists in the poling degree of the porous and monolithic layers within the PSL material. We assume that its porous matrix is fully non-poled, and each grain of the monolithic FC rod is characterised by the domain-wall mobility γ_1 that is constant over the whole porous layer. By analogy with the FC rod, the domain-wall mobility of the monolithic FC layer is γ_2 = constant. Despite the aforementioned reasons, we state that the columnar FC structure in the porous layer represents reliable polarisation paths though the porous inner layer and strongly influences its piezoelectric and dielectric properties (figures 3 and 4).

To compare the calculation results, we used analytical formulae for effective electromechanical properties of the 1–3 [28] and series-connected 2–2 [15] composites based on FCs. The formulae from work [28] were applied to find the full set of electromechanical constants of the porous layer of the PSL on assumption that the properties of the porous matrix were previously determined by using Eq. (4). The formulae from monograph [15] were applied to the laminar structure [figure 1(b)] wherein the electromechanical interaction between the

monolithic and porous layers was taken into consideration. Hereby we state good agreement between the effective properties found for the PSL by different methods: a difference between the similar parameters calculated in different ways is less than 3%.

Based on the piezoelectric and dielectric properties of the PSL $BaTiO_3$, we show the dependence of its squared FOMs $(Q^*_{3j})^2$ on the relative density α (figure 5). Due to validity of Eq. (1), the condition

$$(Q^*_{33})^2 >> (Q^*_{31})^2 \qquad (7)$$

holds. On increasing the volume fraction r and on decreasing the volume fraction m_p, we observe decreasing $(Q^*_{3j})^2$ that is caused by the considerable influence of the piezoelectric coefficients g^*_{3j} on the squared FOMs, see Eqs. (2) and (3). Based on the electromechanical constants of the poled $BaTiO_3$ FC [21], we evaluate its squared FOMs $(Q_{33})^2 = 2.40$ and $(Q_{31})^2 = 0.404$ (in 10^{-12} Pa^{-1}). The squared FOMs evaluated from experimental data on the monolithic FC samples used in the present study are $(Q_{33})^2 = 1.17$ and $(Q_{31})^2 = 0.172$ (in 10^{-12} Pa^{-1}). Thus, the studied PSL structure enables us to increase $(Q^*_{33})^2$ by a few times in comparison to the poled monolithic $BaTiO_3$ FC, and the obtained $(Q^*_{3j})^2$ values obey the condition (7) in the wide α range.

In Table 2 we show the performance of the PSL $BaTiO_3$ with a small difference between γ_1 and γ_2, i.e., when the domain-wall mobility in grains of the monolithic FC components undergoes small changes. It is seen that the

piezoelectric coefficient d_{33}^* is overestimated even at a volume fraction $r \leq 0.1$ of the FC rods, and no $d_{33}^*(\alpha)$ dependence is observed among the calculated values. An average value of d_{31}^* related to $r = 0.10$ and 0.05 is in good agreement with the experimental d_{31}^* value [see figure 2(a)] when α is constant. The dielectric permittivity $\varepsilon_{33}^{*\sigma}$ is smaller than that measured on the PSL sample [see figure 2(b)]. The large d_{33}^* values related to PSL $BaTiO_3$ at $r \leq 0.1$ (see Table 2) suggest that the domain-wall mobility γ_2 of the monolithic layer is to be decreased at the unchanged characteristics of the porous layer.

4. Conclusions

This paper describes a detailed experimental and modelling analysis of the piezoelectric properties, dielectric properties and energy-harvesting parameters of novel porous sandwich layer (PSL) structures based on $BaTiO_3$ containing dense outer layers and inner layer with a porosity of $p_{in} \approx 0.5$–0.6. The experimental study of the microgeometry and physical properties of this lead-free ferroelectric material demonstrate that conditions in Eqs. (1) and (7) are valid in a wide range of the relative density (α). The ability of the structure to achieve a large piezoelectric anisotropy with a high $d_{33}^* \approx 100$ pC / N suggests that this lead-free piezoelectric material has obvious advantages over conventional highly anisotropic $PbTiO_3$-type FCs. The $d_{3j}^*(\alpha)$ and $\varepsilon_{33}^{*\sigma}(\alpha)$ dependences are interpreted in terms of a model of a laminar structure [figure 1(b)] whereby the electromechanical interaction of the

porous and monolithic layers plays a key role in forming the beneficial electromechanical properties and their anisotropy. The porous layer is represented as a piezocomposite with 1–3–0 connectivity, and the system of the monolithic FC rods strongly influences the electromechanical properties of this layer. The difference between the 90° domain-wall mobility levels in grains of the FC components of PSL structures and the presence of the heavily oblate air pores are to be taken into account at the prediction of the piezoelectric and dielectric properties, hydrostatic parameters and squared FOMs. The studied PSL $BaTiO_3$ is characterised by the squared FOM $(Q_{33}^*)^2 \sim 10^{-12}$ Pa^{-1} under longitudinal excitation and by the hydrostatic piezoelectric coefficients $d_h^* \approx 100$ pC / N and $g_h^* \approx 20$ mV·m / N at $\alpha = 0.64–0.70$. The new type of ferroelectric structure proposed here that is based on a lead-free material provides a fascinating route for the design of ferroelectric structures for piezoelectric sensor, energy-harvesting and related transducer applications.

Acknowledgments

The authors would like to thank Prof. Dr. A. A. Nesterov and Prof. Dr. A. E. Panich (Southern Federal University, Russia) for their research interest in the piezoelectric performance of advanced materials. Prof. Dr. C. R. Bowen acknowledges funding from the European Research Council under the European Union's Seventh Framework Programme (FP/2007-2013) / ERC Grant Agreement no. 320963 on Novel Energy Materials, Engineering Science and Integrated

Systems (NEMESIS). Mr. J. I. Roscow acknowledges funding from Engineering and Physical Sciences Research Council (EPSRC), UK. In the present paper, the results on the research project no. 11.1627.2017/4.6 PCh have been represented within the framework of the state task in the scientific activity area at the Southern Federal University, and Prof. Dr. V. Yu. Topolov acknowledges relevant funding. This research has been performed using the equipment of the Centre of Collective Use ‘High Technologies’ at the Southern Federal University.

References

[1] Bowen C R, Perry A, Lewis A C F and Kara H 2004 *J. Europ. Cer. Soc.* **24** 541–5

[2] Praveenkumar B, Kumar H H and Kharat D K 2006 *J. Mater. Sci.: Mater. Electron.* **17** 515–8

[3] Levassort F, Holc J, Ringgaard E, Bove T, Kosec M and Lethiecq M 2007 *J. Electrocer*. **19** 127–39

[4] Lupeiko T G and Lopatin S S 2004 *Inorg. Mater*. **40** Suppl. 1 S19–32

[5] Roscow J I, Taylor J and Bowen C R 2016 *Ferroelectrics* **498** 40–6

[6] Roscow J I, Topolov V Yu, Bowen C R, Taylor J and Panich A E 2016 *Sci. Technol. Adv. Mater*. **17** 769–76

[7] Roscow J I, Lewis R W C, Taylor J and Bowen C R 2017 *Acta Mater.* **128** 207–17

[8] Topolov V Yu and Bowen C R 2009 *Electromechanical Properties in Composites Based on Ferroelectrics* (London: Springer)

[9] Filippov S E, Vorontsov A A, Brill O E and Topolov V Yu 2014 *Funct. Mater. Lett.* **7** 1450029

[10] Lopatin S S, Lupeiko T G, Nesterov A A and Vikhryanova I V 1988 *Inorg. Mater.* **24** 1056–8

[11] Bast U and Wersing W 1989 *Ferroelectrics* **94** 229–42

[12] Dunn M L and Taya M 1993 *J. Am. Cer. Soc*. **76** 1697–706

[13] Topolov V Yu, Glushanin S V and Bowen C R 2005 *Adv. Appl. Cer*. **104** 300–5

[14] Lewis R W C, Dent A C E, Stevens R and Bowen C R 2011 *Smart Mater. Struct*. **20** 085002

[15] Khoroshun L P, Maslov B P and Leshchenko P V 1989 *Prediction of Effective Properties of Piezo-active Composite Materials* (Kiev: Naukova Dumka, in Russian)

[16] Malakooti M H and Sodano H A 2013 *Composites: Part B* **47** 181–9

[17] Hong C-H, Kim H-P, Ghoi B-Y, Han H-S, Son J-S, Ahn C W and Jo W 2016 *J. Materiom*. **2** 1–24

[18] Uchino K 2012 *Lead-free Piezoelectrics*, Eds. Priya S and Nahm S (New York, Dordrecht, Heidelberg, London), p. 511–28

[19] Webber K G, Vögler M, Khansur N H, Kaeswurm B, Daniels J E and Schader F H 2017 *Smart Mater. Struct*. **26** 063001

[20] Ikegami S, Ueda I and Nagata T 1971 *J. Acoust. Soc. Am*. **50** 1060–6

[21] Berlincourt D A, Cerran D R and Jaffe H 1964 *Physical Acoustics. Principles and Methods, Vol. 1, Pt A – Methods and Devices*, Ed. Mason W (New York: Academic Press), p. 169–270

[22] Newnham R E, Skinner D P and Cross L E 1978 *Mater. Res. Bull.* **13** 525–36

[23] Aleshin V I 1990 *Zh. Tekhn. Fiziki* **60** 179–83 (in Russian)

[24] Topolov V Yu and Bowen C R 2008 *Modelling Simul. Mater. Sci. Eng*. **16** 015007

[25] Huang J H and Kuo W-S 1996 *Acta Mater*. **44** 4889–98

[26] Ikeda T 1990 *Fundamentals of Piezoelectricity* (Oxford, New York, Toronto: Oxford University Press)

[27] Wang Y, Hou Y and Deng Y 2017 *Compos. Sci. Technol*. **145** 71–7

[28] Grekov A A, Kramarov S O and Kuprienko A A 1989 *Mechanics of Composite Materials* **25** 54–61

Appendix. List of symbols and abbreviations

a_{1p}, a_{2p} and a_{3p}, semiaxes of the pore

c, coefficient that links the 90° domain-wall displacement and thermodynamic pressure

$|| c^E ||$ is the matrix of elastic moduli measured at electric field E = constant

$|| C^{(FC)} ||$, matrix of electromechanical properties of poled ceramic rods

$|| C^{(m)} ||$, matrix of electromechanical properties of the poled ceramic medium with spheroidal pores

$|| C^{(1)} ||$, matrix of electromechanical properties of the monolithic ceramic

D, electric displacement

d_h, hydrostatic piezoelectric coefficient

d_{ij}, piezoelectric coefficient

E. electric field

$|| e^{(1)} ||$, matrix of piezoelectric coefficients of the monolithic ceramic

e_{ij}, piezoelectric coefficient

g_h, hydrostatic piezoelectric coefficient

g_{ij}, piezoelectric coefficient

H, average width of the 90° domain

$|| I ||$ identity matrix

m, volume fraction of the porous layer, see figure 1(b)

m_p volume fraction of air pores in the ceramic medium, see figure 1(b)

p_{in}, inner layer porosity

$(Q_{31})^2$, squared figure of merit concerned with the transverse piezoelectric effect

$(Q_{33})^2$, energy-harvesting figure of merit, squared figure of merit concerned with the longitudinal piezoelectric effect

r, volume fraction of poled ceramic rods in the porous layer, see figure 1(b)

|| S ||, matrix containing components of the Eshelby electroelastic tensor of the poled ceramic medium

|| $S^{(m)}$ ||. matrix containing components of the Eshelby electroelastic tensor of the non-poled porous ceramic medium

s_{ab}^{E}, elastic compliance at electric field E = constant

t, superscript that denotes the matrix transposition

v_p, porosity of the porous sandwich layer structure, see figure 1(b)

α, bulk relative density of the porous sandwich layer structure

γ, factor that characterises the 90° domain-wall mobility in ceramic grains; γ_1 refers to the domain-wall mobility in grains of the ceramic rod, and γ_2 refers to the domain-wall mobility in grains of the monolithic ceramic layer [see figure 1(b)]

ε_0, dielectric permittivity of free space ($\varepsilon_0 = 8.854 \cdot 10^{-12}$ F m^{-1})

|| $\varepsilon^{(1),\xi}$ ||, matrix of dielectric permittivities of the monolithic ceramic at mechanical strain ξ = constant

$\varepsilon_{pp}^{\sigma}$, dielectric permittivity at mechanical stress σ = constant

ρ_p, aspect ratio of the air pore

σ, mechanical stress

ξ, mechanical strain

1–3–0, 1–3, 3–0, and 2–2, connectivity indexes of composites

Asterisk (*) is used to show effective properties and parameters of the porous sandwich layer or composite

FC, ferroelectric ceramic

FOM, figure of merit

PEG, polyethylene glycol

PSL, porous sandwich layer; PSL-1 and PSL-2 are related to inner layer porosity $p_{in} \approx 0.5$ and 0.6, respectively

SEM, scanning electron microscopy

Table 1. Experimental and calculated values of piezoelectric coefficients d_{33}^*, d_h^* (in pC / N), g_{33}^*, and g_h^* (in mV·m / N) of PSL $BaTiO_3$ at α = const

Sample	PLS-1			PLS-2		
α	0.70	0.72	0.74	0.66	0.72	0.82
d_{33}^*, experimental	110	122	115	121	114	109
d_h^*, experimental	84.1	89.3	86.2	101	90.5	73.2
g_{33}^*, experimental	19.6	18.6	17.6	25.6	20.4	13.9
g_h^*, experimental	15.0	13.6	13.2	21.4	16.2	9.3
d_{33}^*, calculated	132	131	129	133	129	119
d_h^*, calculated	91.4	89.8	86.4	92.6	86.0	67.8
g_{33}^*, calculated	26.1	25.1	23.7	28.9	23.3	17.5
g_h^*, calculated	18.1	17.1	15.9	20.1	15.5	10.0

Note. Calculations of the piezoelectric coefficients were performed within the framework of the model shown in figure 1(b) and by using the averaging procedures described in Section 3. Hereby the following parameters were used: m_p = 0.6, ρ_p = 100, r = 0.20, lg γ_1 = 0, and lg γ_2 = –4 (for PSL-1), and m_p = 0.7, ρ_p = 100, r = 0.20, lg γ_1 = 0, and lg γ_2 = –4 (for PSL-2).

Table 2. Experimental and calculated values of piezoelectric coefficients d_{3j}^* (in pC / N) and relative dielectric permittivity $\varepsilon_{33}^{*\sigma}$ of PSL-2 $BaTiO_3$ at α = const, lg $\gamma_1 = 0$, and lg $\gamma_2 = -1$

α	d_{33}^*	d_{31}^*	$\varepsilon_{33}^{*\sigma} / \varepsilon_0$
Experimental			
0.66	121	–10.0	534
0.72	114	–11.8	631
0.82	109	–17.9	886
Calculated at $m_p = 0.7$, $\rho_p = 100$ and $r = 0.10$ (inner layer porosity $p_{in} = 0.63$)			
0.66	136	–13.2	374
0.72	136	–15.1	431
0.82	134	–19.8	568
Calculated at $m_p = 0.7$, $\rho_p = 100$ and $r = 0.05$ (inner layer porosity $p_{in} = 0.57$)			
0.66	124	–7.0	220
0.72	124	–8.1	252
0.82	124	–11.3	345

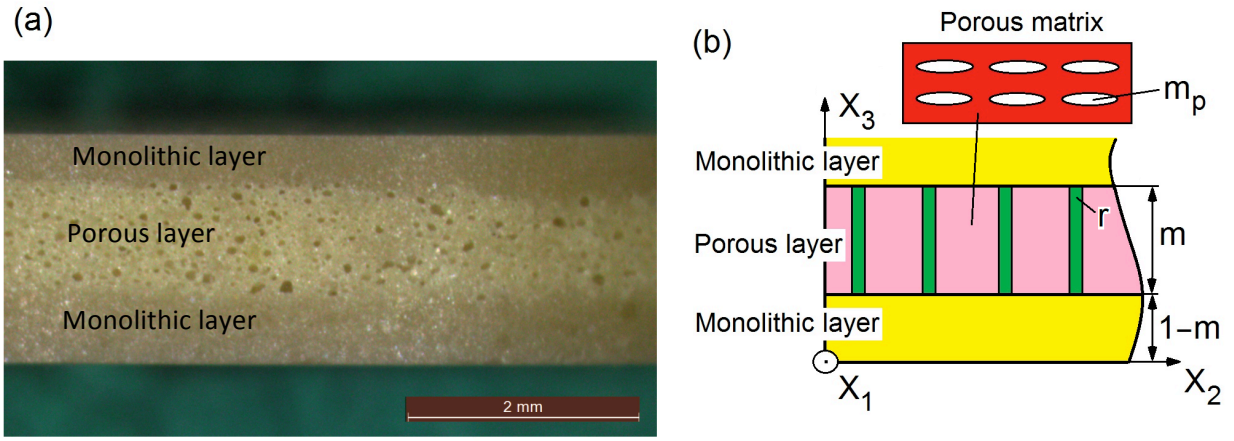

Figure 1. Optical micrograph of PSL $BaTiO_3$ (a) and schematic (b) that is used to describe the electromechanical properties and related parameters of the PSL structures. In the micrograph (a), the porous layer is located between the monolithic FC layers. The PSL sample as a whole has been poled in the vertical direction. In the schematic (b), $(X_1X_2X_3)$ is the rectangular co-ordinate system, m and $1 - m$ are volume fractions of the porous and monolithic layers, respectively, r is the volume fraction of monolithic FC rods in the porous layer, and m_p is the volume fraction of air pores in the matrix (see the inset) that surrounds the monolithic FC rods in the porous layer.

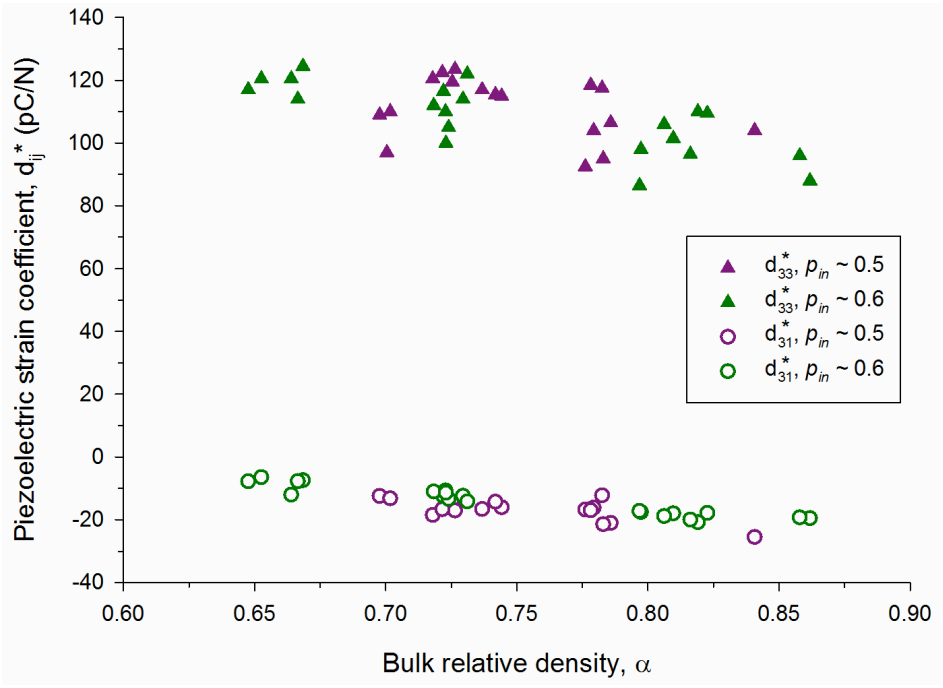

a

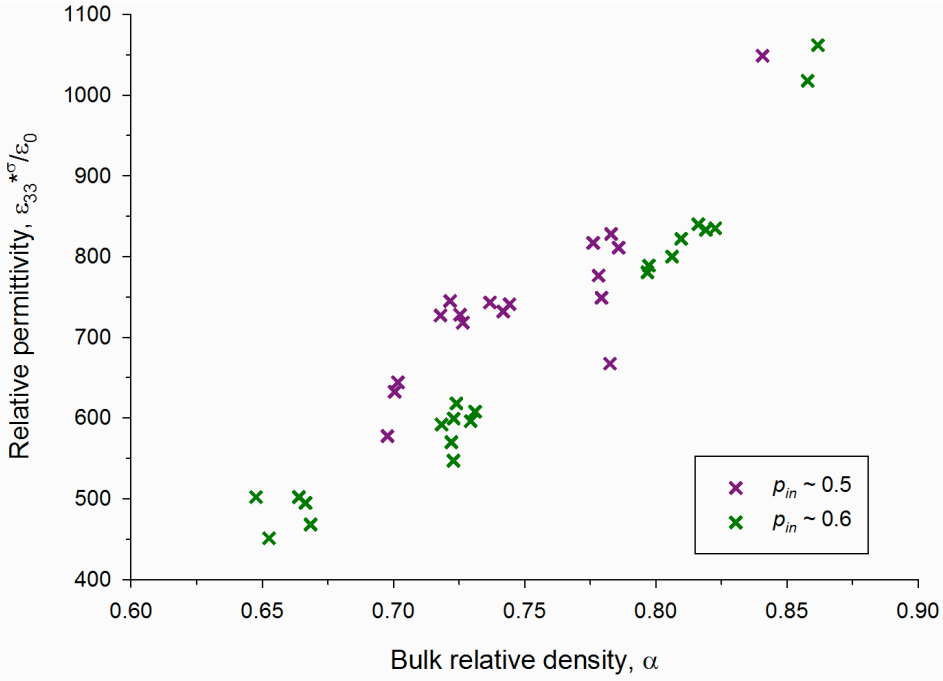

b

Figure 2. Room-temperature piezoelectric coefficients d_{3j}^* and relative dielectric permittivity $\varepsilon_{33}^{*\sigma}/\varepsilon_0$ as functions of the bulk relative density α of PSL $BaTiO_3$ at the the inner layer porosity $p_{in} \approx 0.5$ and 0.6. The relevant layer is shown in the middle part of figure 1(a) and termed 'porous layer' in figure 1(b).

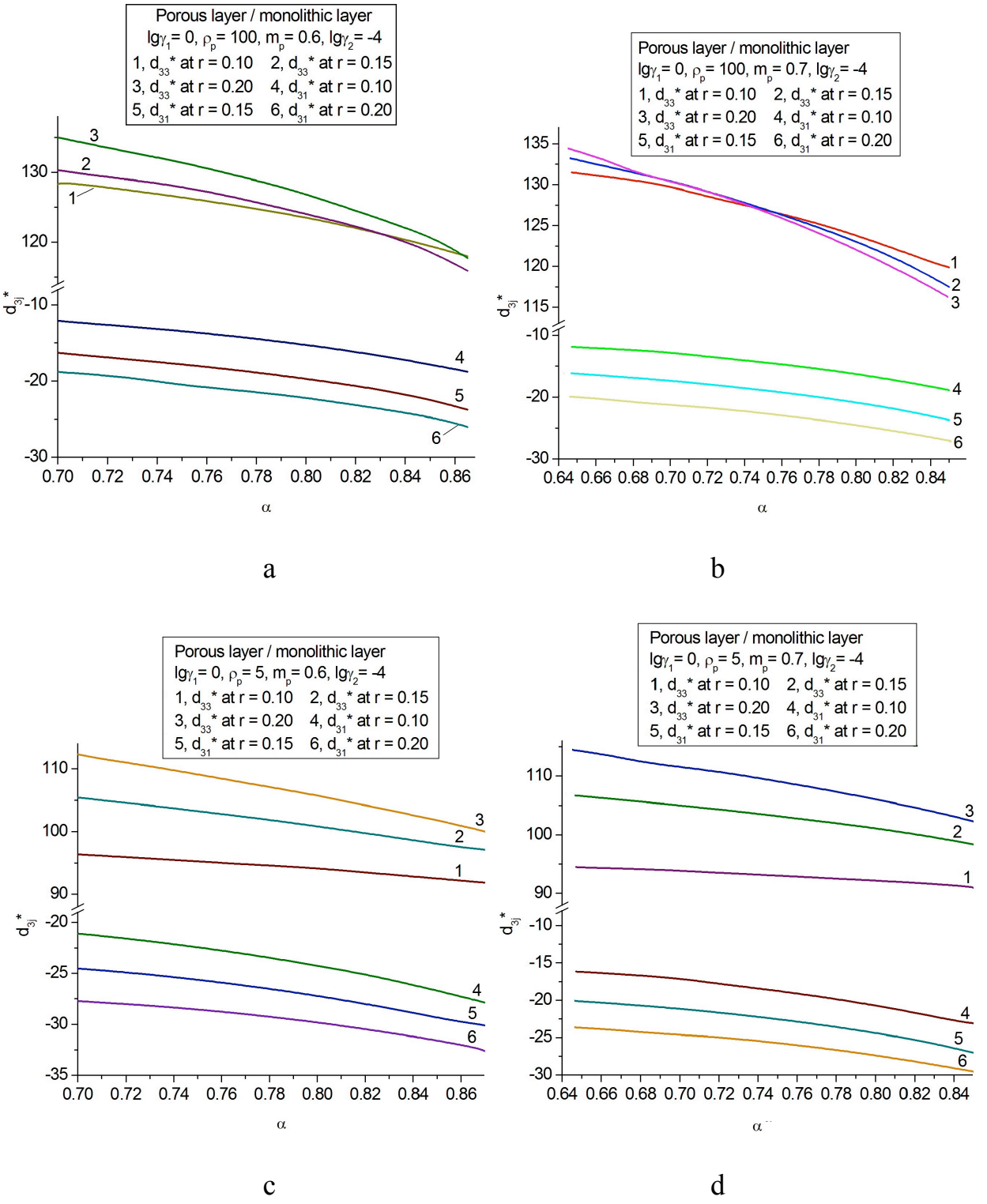

Figure 3. Evaluated piezoelectric coefficients d_{3j}^{*} (in pC / N) as functions of the bulk relative density α of PSL $BaTiO_3$ at fixed volume fractions *r* of the poled FC rods in the porous layer [see the schematic in figure 1(b)].

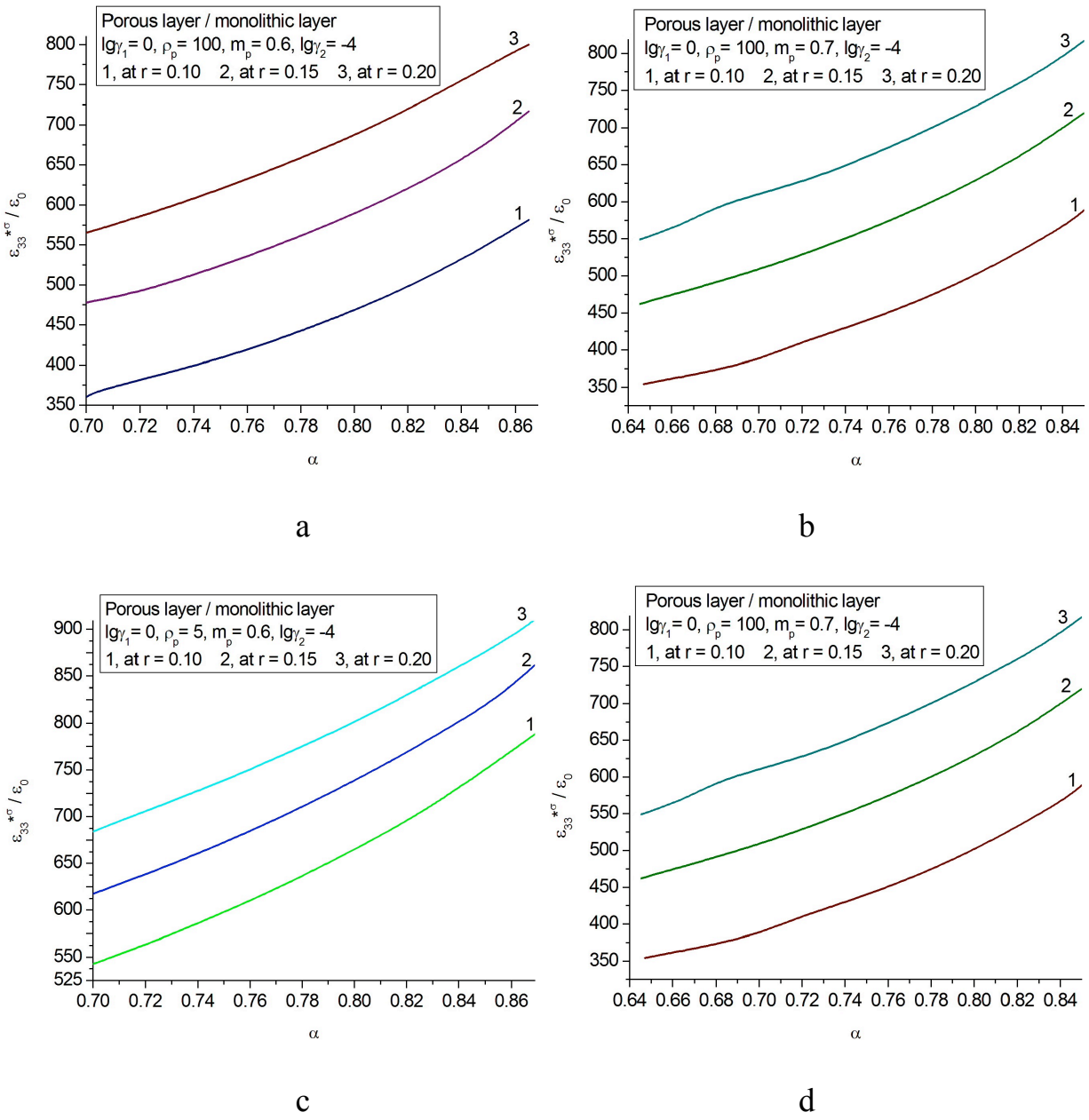

Figure 4. Evaluated relative dielectric permittivity $\varepsilon_{33}^{*\sigma}/\varepsilon_0$ as a function of the bulk relative density α of PSL $BaTiO_3$ at fixed volume fractions *r* of the poled FC rods in the porous layer [see the schematic in figure 1(b)].

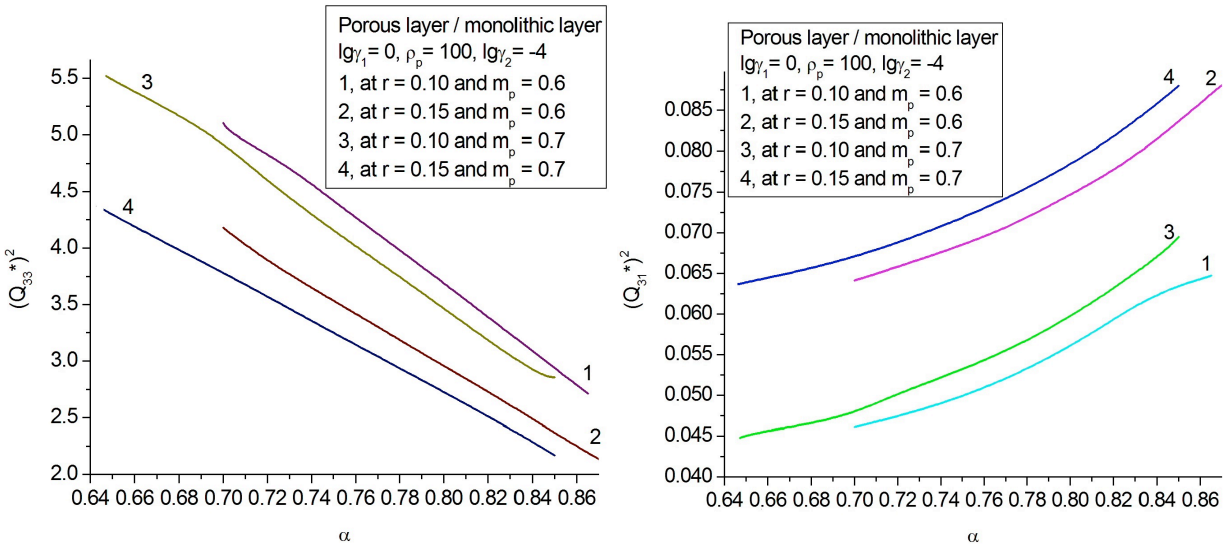

a b

Figure 5. Evaluated squared FOM $(Q_{33}^{*})^2$ (in 10^{-12} Pa^{-1}) as a function of the bulk relative density α of PSL $BaTiO_3$ at fixed volume fractions *r* of the poled FC rods and m_p of air pores in the porous layer [see the schematic in figure 1(b)].